Journal of Power Sources 245 (2014) 915–926

Contents lists available at SciVerse ScienceDirect

Journal of Power Sources

journal homepage: www.elsevier.com/locate/jpowsour

Preparation and characterization of polybenzimidzaole/diethylamine hydrogen sulphate for medium temperature proton exchange membrane fuel cells

M. Mamlouk [a,*], P. Ocon [b], K. Scott [a]

[a] School of Chemical Engineering and Advanced Materials, Merz Court, University of Newcastle, Newcastle upon Tyne NE1 7RU, United Kingdom
[b] Department of Physical Chemistry, University of Autonoma of Madrid, C/Tomás y Valiente n°7, 28049 Madrid, Spain

HIGHLIGHTS

- Dietlyamine bisulphate/sulfate was synthesised and characterised for HT-PEMFCs.
- FTIR spectra showed that ionic liquid did not change the PBI structure.
- PBI/*x*DESH membranes conditions with conductivity >0.01 S cm^{-1} at 150 °C.
- The measured proton conductivity is ca. 4 times lower than ionic conductivity.
- The ionic liquid drag will limit the life of the cell due to the IL migration.

ARTICLE INFO

Article history:
Received 8 March 2013
Received in revised form
28 June 2013
Accepted 10 July 2013
Available online 16 July 2013

Keywords:
Ionic liquid
PBI
HT-PEMFCs
Diethlyamine
Bisulphate
Sulphate

ABSTRACT

Diethlyamine bisulphate/sulphate, an ionic liquid, was synthesised and characterised for high temperature fuel cell applications. Composite hybrid membranes of PBI and the ionic liquid diethlyamine bisulphate/sulfate were fabricated at different composition ratios PBI/xDESH. FTIR spectra showed that the IL did not change the PBI structure. The ionic liquid only weakly interacts with PBI and remains free inside the structure allowing for the observed ionic conduction.

PBI/xDESH membranes could operate under a higher temperature values/low humidity conditions with conductivity >0.01 S cm^{-1}.

The measured proton conductivity, from symmetrical H_2 cell, however, is ca. 4 times lower than that of the measured ionic conductivity. This could be estimated roughly by considering proton conduction where the proton is associated with two anions A^- resulting in ionic agglomerate HA^{2-} with more than double the ionic radius of A^- and consequently less than half of its diffusivity. Additionally, considering the solvation number of that agglomerate to be 1.0 will result not only in a slower proton diffusion and lower conductivity but will also cause serious flooding and mass transport limitation at the cathode. This cumulative effect will limit the life of the cell due to the IL migration from anode and membrane to the cathode.

1. Introduction

Polymer electrolyte membrane fuel cell, PEMFC, using hydrogen and oxygen, directly convert their chemical energy into electrical energy with only water as the by-product. Current fuel cells most often contain polymer electrolyte membranes carrying sulfonic acid groups [1–3]. The main obstacles to the commercial use of perfluorinated polymers for fuel cell applications are cost, efficiency, durability, thermal and mechanical stability and water management [4,5]. Water is essential for the mobility of their protonic charges carriers as it solvates the proton and promotes its mobility by structure diffusion and by vehicle-type transport [6–8]. The conductivities of these membranes rely on maintaining a sufficient hydration level, and thus constant humidification is required and their operating temperature is usually limited to <90 °C. A factor allowing further progress in polymer electrolyte membranes fuel cell is an increase in operational temperature above 100 °C [9], in an ideal case above 150 °C. PEMFCs operating at higher temperatures have a number of benefits: the reaction rate at both electrodes, anode and cathode, is increased, a better CO tolerance allows a

* Corresponding author. Tel.: +44 191 222 5207; fax: +44 191 222 5292.
E-mail address: mohamed.mamlouk@ncl.ac.uk (M. Mamlouk).

0378-7753/$ – see front matter © 2013 Elsevier B.V. All rights reserved.
http://dx.doi.org/10.1016/j.jpowsour.2013.07.050

simplified fuel pre-treatment [10–13], a higher operating ionic conductivity can be obtained and cogeneration of heat and power production becomes possible [14].

Research on membrane development for sustainable high temperature PEMFCs operating under dry conditions is frequently directed towards dense polybenzimidazole (PBI, Poly(2,2′-m-(phenylene)-5,5′-bibenzimidazole)) membranes. PBI is a promising candidate for use in a high temperature environment. It has excellent chemical and thermal stability and it is often used in thermal protective clothing and fire blocking applications. Depending on its grade, PBI has an upper working temperature between 260 °C and 400 °C. Ideally, the electrolyte within these fuel cells would allow operation without humidification with a strong drive to increase the available operating temperatures to at least 120 °C. As with most polymers, PBI is an electrical insulator and many attempts have been made in recent years to improve its proton conductivity. Often PBI is doped with phosphoric acid to provide proton conductivity [12,15,16], but the chemical stability of the PBI membranes rapidly degrades at temperature above 150 °C due to dehydration of phosphoric acid and other environmental issues [17]. It has been reported that oxygen reduction activities of platinum electrodes, in 85% H_3PO_4, was much higher when the oxide layer was removed (by pre-treatment at cathodic potentials) compared to oxidized platinum electrodes. In addition, there would be deactivation with phosphate anion adsorption at positive potentials [16,18]. Besides, acid leaching is another factor that needs addressing. Sulphuric acid [15] and other organic molecules as imidazole and pyrazoles [19] were used in order to improve the ionic conductivity of PBI.

Different authors [19,20] propose the use of ionic liquids (IL) as a conductive electrolyte to replace phosphoric acid with the intention to overcome the disadvantages resulting from the acid. IL, i.e. molten salts at low temperatures <100 °C, have very interesting properties as high temperature electrolytes due to their low volatility, chemical and thermal stability, non-flammability and high ionic conductivity.

The use of IL based membranes as anhydrous electrolyte is well documented in the literature [21–24]. Most of the materials are evaluated in terms of ionic conductivity. With values in the range of 10^{-3}–10^{-2} S cm^{-1}, ILs are claimed to be an alternative for anhydrous fuel cell operation. However, data on their use in fuel cell is very limited. Relying only on ionic conductivity values can be misleading, for a start: there is confusion between the measured ionic conductivity σ_{imp} of IL based composite membranes and their proton conductivity. σ_{imp} is related to the ionicity (dissociation) of the IL. Proton conductivity might be only a fraction of the observed ionic conductivity.

The transport of the charge is mainly ionic rather than protonic in several IL [21], because the ratio of equivalent conductivity to fluidity (Walden Plot) is below the ideal KCl plot, unlike aqueous mineral acids (above KCl) where the transport is assisted by the independent jumping of protons [21].

The molar conductivity ratio $\Lambda_{imp}/\Lambda_{est}$ is a precise physicochemical parameter for representing the self-dissociation of ILs, Λ_{imp} is calculated from the ionic conductivity from impedance measurement and Λ_{est} is the estimated value from the self-diffusion coefficient of cation D^+ and anion D^- given by Nernst–Einstein equation [22]:

$$\Lambda_{est} = \frac{F^2}{RT}\left(D^+ + D^-\right) \quad (1)$$

where F is Faraday constant, R is gas constant, and T is the absolute temperature.

Equation (1) assumes that every diffusing species contributes to the molar conductivity. In contrast, Λ_{imp} relies on the migration of charged species in an electric field. The ratio $\Lambda_{imp}/\Lambda_{est}$, therefore, indicates the proportion of ions that contribute to ionic conduction from all the diffusing species and can be used as a quantitative measure of ionicity [22]. When the association of anions and cations is predominant, in which charges are completely neutralized $\Lambda_{imp}/\Lambda_{est}$ will show very low value. Although ideal ILs consists of non-associated ions, in reality they form aggregates or clusters to some extent. There is experimental evidence of ionic association in ILs [22]. The increase in the cohesive energy and consequently the extremely low vapour pressure of ILs is a result of predominant coulombic interactions, short distance interaction, between the anion and cations leading to $\Lambda_{imp}/\Lambda_{est}$ values below 1.

In amine based protic ILs, the acceptor of the proton generated by the HOR is either amine [23,24] (Reaction (2)) or the anion as shown in Reaction (3), or if the used anion is relatively a strong acid that can further ionize to release another proton such as HSO_4^- ($pK_a = 1.99$ at 25 °C) as of Reaction (4). The protonated product of Reactions (2), (3) or (4) will diffuse to the cathode and react with O_2 to produce water (Reaction (5)) for the case of Reaction (3) or Reaction (6) for the case of Reaction (2):

$$R' - NH - R + H^+ \leftrightarrow R' - NH_2^+ - R \quad (2)$$

$$4A^- + H_2 \leftrightarrow 2HA_2^- + 2e^- \quad (3)$$

$$HB^- + H_2O \leftrightarrow H_3O^+ + B^{-2} \quad (4)$$

$$2HA_2^- + 2e^- + \frac{1}{2}O_2 \rightarrow H_2O + 4A^- \quad (5)$$

$$R' - NH_2^+ - R + 2e^- + \frac{1}{2}O_2 \rightarrow H_2O + R' - NH - R \quad (6)$$

In anhydrous systems, Reaction (3) is the most likely to occur as the degree of dissociation in Reaction (2) is very small ($pK_a = 10.68$ at 25 °C) and Reaction (4) become negligible without water. However diffusion of HA_2^- is much slower than that of A^- (less than half by simply using the Stokes–Einstein equation). Moreover, interactions between the solute (H^+) and the dipolar solvent (IL), result in a number of solvent molecules orientating themselves around each solute molecule, forming a complex aquo-ion (hydration shell) equal to 4 for H^+ in H_2O [25]. This increase in ion radius due to solvation will result in decrease in conductivity accordingly allowing for the calculation of the solvation number even in nonaqueous solution, for example: Li^+/Methanol equal to 7 [26]. Li^+/N-methylacetamide and H^+/N-methylacetamide equal to 5 and 3, respectively [27].

While most of the attention in current research is focussing on the ionic conductivity, the suitability of the electrolyte for fuel cell application is of paramount importance, this includes: proton transport number (conductivity), thermal stability, dimensional stability with changes in temperature and hydration, electrochemical stability on Pt (under reducing and oxidizing potentials in the presence of O_2 and H_2). The compatibility with the electrocatalyst in the fuel cell is also critical (its performance can be significantly impacted by loss of contact or adsorption of the IL material [28]). The conducting salt significantly affects the reversibility and kinetics of oxygen reduction in non-aqueous electrolytes [29].Viscosity also strongly influences mass transport of electroactive species hence determining kinetics of the reaction [29].

The low open circuit voltage could arise from the IL anion adsorption on the noble catalyst or its electrochemical activity as an intermediate in Reactions (2) and (5) above or due to a mixed potential arising from electrochemical instability of the IL ions

(reduced or oxidized). The possible influence of solvation layers, or more generally of adsorbed ionic liquids specially in non-aqueous solutions, on electrochemical processes has hitherto been neglected in the literature [30]. In aqueous solutions, ion adsorption on a metal surface is favourable when the ion adsorption free energy is less than that of water, however in the absence of water, adsorption of even typically low adsorbing large anions such as trifluoromethanesulphonate becomes significant. The catalytic activity of Pt for oxygen reduction reaction (ORR) in a mixture of bis (trifluoromethane sulphonyll) imide and 1-ethyl-3-methylimidazolium bis (trifluoromethane sulphonyll) imide decreased with time because of adsorption of the TFSI anion [31].

The adsorption of various IL on Au(111) is reported [32]. It was shown that the innermost layer is enriched in ions that interact electrostatically with the gold surface. This layer contracted and became harder to displace (more tightly bound) as the surface potential was increased. The presence of an adsorbed layer of IL (1-butyl-1-methylpyrrolidinium bis(trifluoromethylsulphonyll) amide or 1-ethyl-3-methylimidazolium bis(trifluoromethylsulphonyll) amide) in nonaqueous conditions is confirmed on Au (111), while a clean surface is observed in aqueous solution of the IL under what are otherwise the same conditions [30].

Platinum has a relatively low hydrogen oxidation reaction (HOR) activity and oxygen reduction reaction (ORR) activity in diethylmethylammonium bis(trifluoromethane sulphonyll)imide environment (inhibitor) and thus the open circuit voltage (OCV) was low at ca. 0.7 V [24]. A H_2/O_2 fuel cell utilizing diethylmethylammonium trifluoromethanesulphonate [dema][TfO] IL showed decreasing OCV values with increasing temperature with a value of ca. 0.7 V at 140 °C and limiting current density of 100 mA cm^{-2} [24]. Limiting current density of 2 and 16 mA cm^{-2} were reported at 100 °C for ORR and HOR, respectively in alkylpiperidinium, combined with fluorohydrogenate anions [33]. An OCV of 0.85 V and limiting current density (j_L) of 0.6 mA cm^{-2} was reported at 130 °C in imidazole- bis(trifluoromethanesulphonyll) IL [34]. OCV of 0.58–0.59 V and j_L of 6 mA cm^{-2} were reported with 1 mg_{pt} cm^{-2} at 100 °C in N-ethyl-N-methylpyrrolidinium [35]. An OCV of 0.7–0.85 V and j_L of 0.6–0.8 mA cm^{-2} at 150 °C 0%RH were reported for bezimidazole/H-bis(trifluoromethanesulphonyl)imide [36]. Recently, OCV of 0.5–0.62 V was reported for porous PBI film with 1-H-3-methylimidazolium bis(trifluoromethanesulphonyll) imide using 5 mg_{pt} cm^{-2} at 1.5 atm pressure and temperature range of 30–150 °C [37]. The OCV was reported to fall from 0.9 to 0.6 V when the temperature was increased from 80 to 120 °C in N-ethyl-N-methylpyrrolidinium fluorohydrogenate (1 mg_{Pt} cm^{-2}) [35]. OCV of 0.58 V and j_L 6 mA cm^{-2} using 1 mg_{Pt} cm^{-2} at 100 °C in 2,3-dimethyl-1-octylimidazolium triflate [38]. OCVs of 0.6 and 0.85 V at 2.5 and 5 mg_{pt} cm^{-2}, respectively, at 120 °C were reported in diethylmethylamonium triflate, with increase to 0.9 V upon the addition of 5% H_3PO_4 enhancing the proton conductivity [39].

The very low limiting current values mentioned earlier in IL based fuel cells does not correspond to the H_2 and O_2 permeability reported in the literature. For example, H_2 and O_2 permeability in solfunated polyimide filled with IL [dema][TfO], at 0%RH were 6×10^{-12} and 6×10^{-13} mol cm cm^{-2} s^{-1} atm^{-1} at 80 °C, respectively [24]. These values are similar to that of dry Nafion and an order of magnitude lower than that of PBI-5H_3PO_4. H_2 and O_2 permeability at 0%RH and 80 °C of 14.4×10^{-12} and 4.1×10^{-12} mol cm cm^{-2} s^{-1} atm^{-1} is reported for Nafion [40] and 120×10^{-12} and 30×10^{-12} mol cm cm^{-2} s^{-1} atm^{-1} for PBI-5H_3PO_4 [41], respectively.

The diffusion coefficient and the solubility of oxygen in diethylmethylammonium trifluoromethanesulphonate[dema][TfO] are reported to be 2.7×10^{-5} cm^2 s^{-1} and 2.3×10^{-3} M at 120 °C, respectively. Those of hydrogen were a factor of 10 and one-tenth compared to oxygen, respectively [42]. The hydrogen evolution reaction showed diffusion limiting current in IL although a diffusion limiting current never appeared in the aqueous electrolyte or upon addition of 10%H_3PO_4. The limiting current was three orders of magnitude lower than that estimated from the permeability, and the diffusion limiting species is the hydrogen carrier species because of the [dema] cation's weak activity for the proton donor. The Li diffusion process in IL was similarly shown to dominate the observed limiting current (along with the toutousity and porosity of the separator film) in binary Li-trifalte based ionic liquid evaluated using symmetric cell Li|IL|Li [43,44].

In this work, in order to assess diethlyamine bisulphate/sulphate ionic liquid for high temperature fuel cell application, we have fabricated composite hybrid membranes of PBI and ionic liquid diethlyamine bisulphate/sulphate, PBI/*x*DESH. The ratio of diethylamine/sulphuric acid was 1/1 mol DESH or 1/2 mol DESH(2).

The addition of excess acid into the IL composite membrane supplies more protons (from acid ionization) and also decreases the viscosity of the ionic liquids. The addition of acids having common anions (with IL) to some extent into polymer/ionic liquid based composite membranes will be a good approach to prepare ionic liquid based composite membranes for anhydrous and high temperature PEMFCs [45]. Sekhon et al. reported that the addition of acids containing a common anion of ionic liquids into the ionic liquid based composite membranes increased ionic conductivity of the composite membranes [38]. In contrast, it was reported that the addition of extra acid to IL (triflate based) did not result in an increase in ionic conductivity; on the contrary, the conductivity of the doped system is lower in the low temperature phases. This indicates a more ordered or less defective phase, either as a result of an ordering effect of the triflic acid or a filling of the anion vacancies [28].

The thermal stability, ionic conductivity, nature of interaction between IL and membrane support is reported in this work. Furthermore, the suitability of the composite membranes for HT-PEMFCs in a single-cell was examined under different conditions.

2. Experimental

2.1. Materials

Diethylamine 99.5%, dimethyl sulfoxide (DMSO) 99.5% and sulphuric acid 96% (Aldrich) were used as received. Poly(2,2′-m-(phenylene)-5,5′-bibenzimidazole) (PBI) powder (BETWEEN, Lizenz GMBH) was dissolved in DMSO at a temperature of 150 °C. Other chemicals and solvents were used as received.

Diethylamine sulphuric acid, (DESH) was prepared by direct neutralization between the Brønsted acid (sulphuric acid) and base (diethylamine). The synthesis was performed in a 50 ml flask under vigorous stirring with 5 or 10 ml of diethylamine, and sulphuric acid was added drop wise till the ratio of diethylamine/sulphuric acid was 1/1 mol or 1/2 mol DESH(2). The temperature was kept at 0 °C using an ice bath. After the reaction, the excess diethylamine and the water were separated by distillation. Upon cooling the ionic liquid, a white solid gel was obtained.

2.2. Preparation of PBI/DESH hybrid membranes

The composite membranes were fabricated using a solution casting method. An appropriate amount of ionic liquid DESH was added to the PBI/DMSO solution (5 wt%), resulting in a viscous solution after stirring. The mixture was sonicated for several hours and placed in a water bath at 75 °C for 12 h. The resulting viscous solution was casted on a Petri dish in an open oven at 80 °C for 12 h. These uniform composite hybrid membranes were peeled from the

Petri dish and dried in an oven at 110 °C for 4 h before starting the measurements. The PBI/*x*DESH membranes, where *x* is the moles of DESH per mole repeat unit of PBI, chosen for this study were 1/3, 1/4, 1/6, 1/8, 1/10 and 1/12.

Membranes obtained by an impregnation method were also studied. PBI membranes obtained from PBI/DMSO solution 5 wt%, were immersed in pure DESH and kept in a water bath at 75 °C for 48 h. The resulting membranes had very low conductivity, practically the same as pristine PBI, as no IL uptake (no increase in weight after doping) was observed.

2.3. Membrane characterization

FTIR spectra of the membranes samples were measured in reflection mode with a Simazu (IRAffinity-1) spectrometer in the range of 4000–500 cm^{-1} with a resolution of 4 cm^{-1}. The KBr pellet method was employed.

^1H MAS NMR spectra were recorded using a Bruker Av-400-WB machine. A triple channel probe (4 mm) with a HR rotor of 40 μL was used. The spectral width was fixed to 50 kHz, with a π/2 at 70 kHz pulse and relaxation time equal to 2 s. The rotational speed was 5 kHz. ^1H was referred to H_2O as a secondary reference, to 4.77 ppm relative to TMS as a primary reference.

The elemental analysis was conducted in silver capsules using a LECO Elemental Analyzer CHNS-932 at an oxidation furnace temperature of 1000 °C and a reduction furnace temperature of 650 °C. The oxygen first and second dosing rates were 20 and 10 cc min^{-1}, respectively.

The mechanical strength of the membranes was measured with a vertical filament stretching rheometer, in which the bottom plate was stationary and the upper plate was pulled at a constant separation rate of 5 mm per minute.

Thermal stability of the PBI, ionic liquids and hybrid membranes was investigated by thermogravimetric analysis (TGA) (TA Instrument 20). The samples were heated from room temperature to 600 °C with a heating rate of 10 °C min^{-1} under nitrogen atmosphere. Weight loss was measured and reported as a function of temperature. Differential scanning calorimetric (DSC) was performed (TA Instrument 10) under nitrogen atmosphere. The samples were tightly sealed in aluminium pans. The samples were first cooled from room temperature to −85 °C and then heated to 250 °C, at 10 °C min^{-1}. The glass transition temperature, T_g, were defined as mid-temperatures of the heat capacity changes.

2.4. Conductivity

Through plane ionic conductivities of the composite membranes were determined by means of complex impedance analysis in the temperature range of 25–200 °C. The two point technique (through plane) used two platinum probes (25 mm × 5 mm) in contact with opposite sides of the measured material. The probes were used to source current and measure the voltage drop.

The electrochemical measurements were carried out with a frequency response analyzer (N4L model PSM1735). The frequencies were swept from 200 kHz to 1 Hz recording six points per decade with AC signal amplitude of 10 mV. The relative humidity was obtained from an intrinsically safe humidity sensor (Vaisala HUMICAPVR, Finland). The conductivity (σ) was calculated as follows:

$$\sigma = \frac{L}{RA} \tag{7}$$

where *R*, *L*, and *A* are the measured resistance, membrane thickness, and cross-sectional area of the membrane, respectively. The membranes were dried in an oven at 110 °C for 4 h followed by further 20 min in-situ drying using dry Argon at 110 °C prior to testing. The dry measurements were carried out between 60 and 120 °C beyond which different humidities were introduced in the temperature range of 120–200 °C.

2.5. Fuel cell

Fuel cell tests were carried out in 1 cm^2 titanium cell with a serpentine flow fields. Mica filled PTFE inserts were used to surround the flow fields and provide location for the O-ring seal. The temperature of the cell was controlled by thermostatically controlled cartridge heaters inserted into the cell body. An Autolab PGSTAT 30 (Eco Chemie, The Netherlands) was used to carry out the electrochemical measurements. Polarization curves were recorded using a cathodic sweep at a scan rate of 0.5 and/or 5 mV s^{-1}.

The catalyst ink was prepared by sonicating the Pt (40%Pt/C Johnson Matthey HiSPEC™ 4000) catalyst and polytetrafluoroethylene (PTFE) dispersion (60 wt% Aldrich) in a water–ethanol mixture. Gas diffusion electrodes (carbon cloth) incorporated with wet proofed micro porous layer obtained from Freudenberg (FFCCT, Germany) was used as substrates to deposit the catalyst layer for both anode and cathode. Typical anodes and cathodes were prepared using 0.3 mg_{Pt} cm^{-2} with 40% wt PTFE.

3. Result and discussion

3.1. Characterization of ionic liquid

The elemental analysis of ionic liquid was done from wet and dry samples. The weight % obtained for carbon C, hydrogen H, nitrogen N and Sulphur S are given in Table 1.

Results from elemental analysis (Table 1) suggest that the ionic liquid DESH or DESH(2), did not simply contain the anion bisulphate (SO_4H^-), rather we could think of it as a mixture of bisulphate and sulphate anions. The ratio value of S/N is 2.29 for pure diethylaminebisulphate (HSO_4^-) or 1.14 for ($SO_4^{=}$) for pure diethylaminesulphate, respectively. However, the experimental S/N ratios obtained were 1.51 to (DESH) and 1.68 to (DESH(2)), suggesting a mixture of both anions.

^1H MAS NMR spectra from both DESH and DESH(2) dry samples were obtained (Fig. 1). The chemical shift results were: δ(ppm) 1.2 (s, 6H), 3.0 (s, 4H), 8.4 (s, 2H from NH) and 10.8 (s, 0.4H from HSO_4^- [46]) for DESH and 1.2 (s, 6H), 3.0 (s, 4H), 8.6 (s, 2H from NH) and 11.4 (s, 0.4H from HSO_4^-) for DESH(2).

According to these results, the integration of the H peak from the bisulphate anion spectrum corresponds to value less than one. This agrees with the earlier indication that mixtures of anion sulphate and bisulphate are present in both DESH and DESH(2). Therefore it was not possible to conclude that the ionic liquid is only a bisulphate diethylamine, but a mixture of sulphate and bisulphate diethylamine.

Table 1
Elemental analysis.

Element	DESH weight %		DESH(2) weight %	
	Wet	Dry	Wet	Dry
C	28.79	32.59	30.55	31.32
H	9.00	8.48	8.34	8.37
N	8.45	9.52	8.87	9.19
S	12.78	14.50	14.81	15.38
S/N	1.51	1.52	1.67	1.67

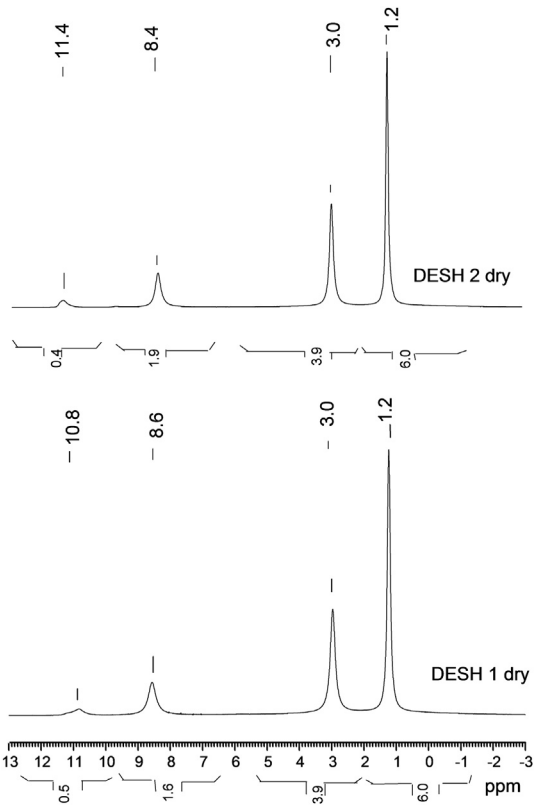

Fig. 1. ^{1}H NMR spectra for dry samples of DESH(1) and DESH(2).

3.2. Characterization of PBI/xDESH hybrid membranes

3.2.1. Infrared study

FTIR spectra of the pure PBI, DESH and PBI/*x*DESH hybrid membranes are shown in Fig. 2. For pure PBI, the peaks corresponding to the free N–H stretch and N–H···H hydrogen bond interaction can be found in the region 3500–2500 cm^{-1}. According to the results of Musto [47,48] absorption peaks situated at 3415 cm^{-1} was attributed to the stretching vibration of isolated nonhydrogen bonds NH group and the very broad peak located between 3100 and 3350 cm^{-1}, approximately centred at 3145 cm^{-1} was assigned to the self associated hydrogen bonded N–H groups. The shoulder at 3063 cm^{-1} was attributed to the stretching modes of aromatics CH groups. PBI blended with DESH, showed a similar peak around 3145 cm^{-1}(to pristine PBI) indicating no hydrogen bonding between bisulphate (HSO_4^-) from the ionic liquid and the "free" nitrogen side of the heterocycles in PBI. Moreover, the intense bands in the FT-IR at 2500–2700 cm^{-1}, characteristic of the PBI acid doped membranes and assigned to the $\nu(N^+–H)$ stretching mode are not visible [49,50]. This agrees with the earlier observation that no IL uptake was observed in the impregnation method (Section 2.2).

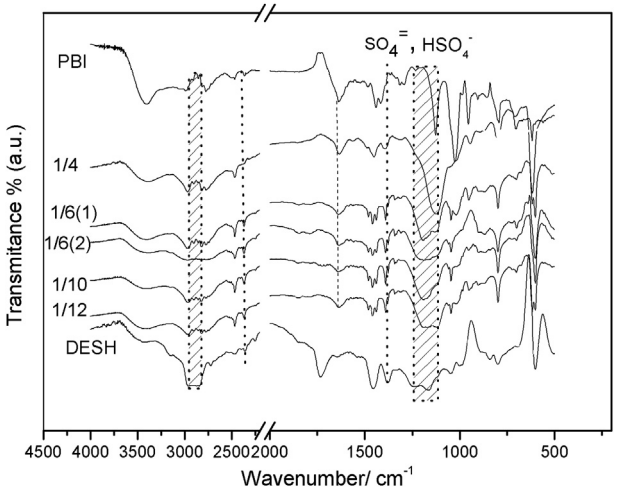

Fig. 2. FTIR spectra of pure PBI, DESH and PBI/*x*DESH hybrid membranes.

For pure DESH the broad peaks located between 3000 and 2841 cm^{-1} represents the stretching of C–H alkyl groups. These peaks were visible in the hybrid membranes incorporating DESH and became more intense with increased amounts of DESH ($x = 4$, 6, 10–12).

In the region 2000–1000 cm^{-1}, the pure PBI spectrum is composed of relatively narrow peaks, due to cycle vibrations as well as in plane NH and CN deformation modes (δNH and δCH). Bands derived from aromatic C=C and C=N stretching modes are found in 1620–1440 cm^{-1}. If the imide groups are protonated, frequency of some of the ring vibrations ν(C–N) located at 1630 cm^{-1} and ν(C–C) at 1534 cm^{-1} at the imidazol ring could decrease. However, this was not observed in the PBI/*x*DESH hybrid membranes case, indicating that the imide groups at the imidazole ring are not protonated in agreement with the earlier conclusion.

The intense absorption bands in the 1300–500 spectral region are characteristics of the sulphur/bisulphate anions from the DESH (Fig. 2), the peaks at 1375 cm^{-1} (ν(S=O_2) H_2SO_4), 1249 cm^{-1} (δ(OH)),1164 cm^{-1} (ν(S=O)HSO_4^-), 1045 cm^{-1} (ν(S::O)HSO_4^- and $SO_4^=$), 602 cm^{-1} ($\nu(SO_4^=)$ and $\delta(SO_3)HSO_4^-$) can be assigned to the species indicated in parenthesis [51]. The C–H out-of-plane vibration, heterocycling-ring vibration and benzene-ring vibration are also seen in this region. It can be concluded that the 1249, 1164 cm^{-1} corresponding to the IL are present in all PBI/*x*DESH hybrid membranes and became more visible with increased amount of *x*DESH.

In summary the ionic liquid incorporated in the PBI, did not change the PBI structure, the imine group from the imidazole ring was not protonated, and the ionic liquid only weakly interacts with PBI and remains free inside the structure of PBI film allowing for the observed ionic conduction.

3.2.2. Thermal properties

The thermal stability of polymer electrolyte membranes was studied at the intended operating temperature range above 100 °C. Fig. 3 shows the thermogravimetric curves of pure PBI, DESH(2) and PBI/*x*DESH hybrid membranes. For pure PBI dried for 4 h at 110 °C, a weight loss of 3% appeared around 200 °C and can be related with small traces of DMSO (solvent) remaining in the membrane (DMSO was detected also by NMR). The 18% weight loss at 600 °C can be attributed to the degradation of the polymer and the residue weight at 850 °C was approximately 71.3%. When the sample was evaluated without prior drying, approximately 1.8% weight loss from room temperature to 120 °C was recorded due to the loss of water in the PBI. The hydroscopic properties of the ionic liquids DESH(2) is reflected in an observed weight loss of 2.7%. Similarly, the produced hybrid membranes PBI/*x*DESH had weight loss of 13.4 and 13.4% for PBI/6DESH(2) and PBI/8DESH, respectively.

The sharp weight loss shown by DESH and DESH(2), of approximately 90%, around 250 °C, could represent the decomposition of the ionic liquid, it is possible that both the aliphatic part of the hydrocarbon and the amine decompose/disappear at this temperature. Weight loss between 120 and 200 °C in the case of PBI/6(DESH(2)), PBI/8DESH and PBI were only 5, 3 and 0.4%,

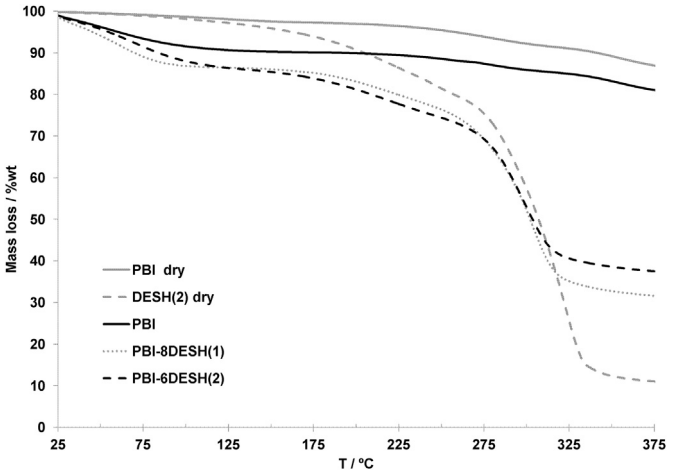

Fig. 3. Thermogravimetric curves for PBI (dry, wet), DESH, DESH(2) and PBI/*x*DESH wet hybrid membranes.

respectively, in the same temperature range restricting their use at temperatures above 200 °C.

Fig. 4 shows the differential scanning calorimetry, DSC thermograms of the pure ionic liquid DESH, DESH(2) and PBI/*x*DESH hybrid membranes. For the pure DESH, a low glass transition temperature of T_g (−54.4 °C) was observed, devitrification (crystallization) temperature T_c around (10.0 °C) and melting point of T_m (53 °C). DESH(2), on the other hand, showed only two values of T_g (−57.4 and 23.8 °C), the first one located very closely to the DESH. The low glass transition temperature is a good indication that the ionic liquid DESH and DESH(2) are likely to have low viscosity and high ionic conductivity. T_g gives a representation of the cohesive energy of the sample, so low T_g values correspond to low cohesive energies. This energy decreases by the repulsive Pauli interaction due to the overlap of closed electron shells, and it increases through the attractive Coulombic, van der Waals and hydrogen-bonding interactions [52].

On the other hand, no significant phase transition was detected in the studied hybrid membranes samples PBI/*x*DESH suggesting no significant interaction between the IL and PBI. Only two T_g

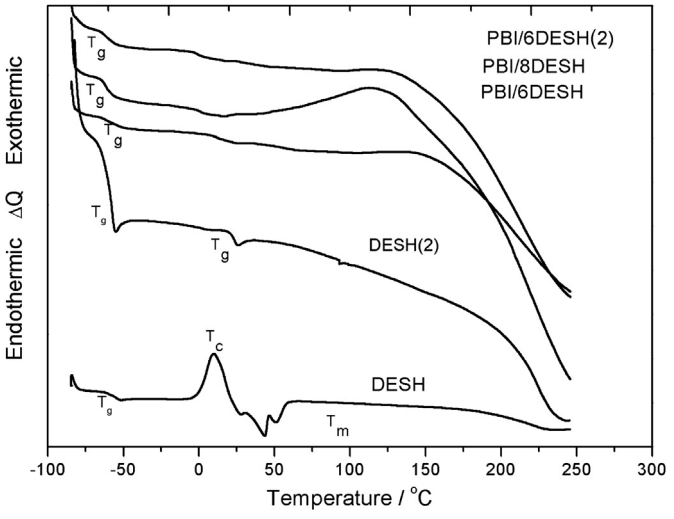

Fig. 4. DSC traces for DESH, DESH(2) and PBI/*x*DESH without prior drying hybrid membranes.

(T_{g1} −61.3, −61.0& −61.6 and T_{g2} +11.2, 0.3 & −1.1 °C) were distinguished for PBI/6DESH, PBI/8DESH and PBI/6DESH(2), respectively. Pure PBI has a glass transition temperature above 400 °C [53].

3.2.3. Conductivity and mechanical properties

Proton transport in ionic liquids is clearly affected when the ionic liquid is mixed with a polymer, such as PBI, generating a hybrid compound. The relative amount of cation and anion diffusion, for example, has been found to change drastically upon incorporation of ionic liquid into a homopolymer and block copolymer. Specific interactions or the prevalence of anionic aggregates cause the cation to diffuse significantly faster (3–4 times) than the anion, which is in contrast with the neat ionic liquid [54].

Pristine PBI has a negligible conductivity and requires doping with acid or IL to facilitate proton conduction. The higher the doping level used, the higher the conductivity. However, the mechanical properties and tensile stress of PBI deteriorate dramatically on increasing the doping level.

The stress at break for phosphoric acid doped PBI is reported to be 130, 48, 30, 7 and 3.5 MPa (decreasing sharply) with an increase in doping amounts (x) of 0, 2.3, 3.3, 5.6 and 6.7, respectively [41]. Similarly, the stress at break for the samples with different doping level is reported. At IL: PBI molar ratios of 0, 4, 6, 10 and 12, the breaking stresses were 138, 10, 2, 1.4 and 0.72, respectively.

The application of the doping acid results in volume swelling of the PBI membranes and therefore an increased separation for the PBI backbones, which in turn would reduce the intermolecular forces and consequently reduce the mechanical strength of the membranes. A balance between good conductivity and mechanical properties is typically achieved at a doping level of around 6 mol of acid/IL per mole of polymer (PRU) [55]. Fig. 5 shows the conductivities of PBI/DESH hybrid membranes at different temperatures and different molar ratio under anhydrous condition between 60 and 120 °C and under different humidifications between 120 and 200 °C. The conductivities of the PBI/*x*DESH hybrid membranes increased with both the temperature and the *x*DESH content. In the dry state and room temperature, pristine PBI has a conductivity of 10^{-5}–10^{-6} S cm^{-1}, while the dry PBI/*x*DESH membranes showed ionic conductivity of 10^{-3} S cm^{-1} with PBI/DESH molar ratios between 1/4 and 1/12. All the ionic conductivities of PBI/*x*DESH hybrid membranes were over 2×10^{-3} S cm^{-1} under hydrous state, at room temperature (not shown in Fig. 5). In comparison Nafion® 117 at 25 °C under hydrous state out performs the dry and humidified PBI/*x*DESH membranes, with proton conductivity of 12×10^{-3} S cm^{-1}. But under dry conditions, Nafion® shows very poor proton conductivity ca 10^{-5} S cm^{-1} [56]. The conductivities of PBI and the PBI/*x*DESH membranes were also measured at higher temperatures, between 60 °C and 120 °C (dry conditions) and 120–200 °C in low humidity conditions, (results are shown in Fig. 5). PBI/*x*DESH membranes showed an ionic conductivity four orders of magnitude higher than that of pristine PBI membrane (1–2×10^{-6} S cm^{-1} at 120–200 °C). The ionic conductivity of the hybrid membrane significantly increases with increased temperature and ionic liquid content and reaches a maximum value of 0.04 S cm^{-1} at 200 °C in PBI/12DESH membrane. The ionic conductivity can be fully attributed to the DEHS ionic liquid incorporated in the hybrid membrane. The results also show that the manufactured hybrid membranes can withstand temperatures up to at least 160 °C without losing their conductivity. The increase of the ionic liquid conductivity with temperature, is possibly due to the decrease in viscosity at higher temperatures. According to the hole theory for transport properties in molten salts, an Arrhenius type Equation (8) for the temperature dependence of the electrical conductivity is expected [57,58].

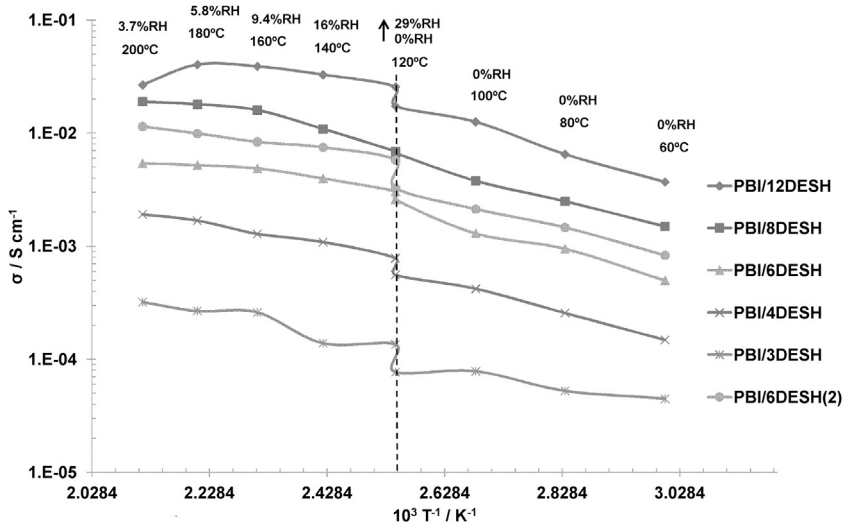

Fig. 5. Temperature dependence of the ionic conductivity of PBI/*x*DESH membranes under anhydrous condition 60–120 °C and hydrous conditions 120–200 °C.

$$\sigma = \sigma_0 \exp\left(-\frac{E_a}{RT}\right) \quad (8)$$

where E_a is the activation energy for electrical conduction (which indicates the energy needed for an ion to jump to a free hole), σ_0 is the maximum electrical conductivity (that it would have at infinite temperature), and R is the gas constant.

All the tested hybrid membranes showed similar temperature dependent conductivity which indicates a similar ionic conductivity mechanism. The slope is linearly fitted from the log (ionic conductivity) with inverse temperature. Table 2 lists the various Arrhenius parameters of PBI/*x*DESH, i.e. slope from regression result, and ionic conduction activation energy.

The activation energy obtained of the PBI/*x*DESH hybrid gel membrane ranges from 16 to 33 kJ mol^{-1} for the membranes under dry conditions (60–120 °C) and from 20 to 26 kJ mol^{-1} for the 60–200 °C dry-humid temperature range, as was indicated in Table 2. The values calculated are similar to the Grotthuss mechanism activation energy, which ranges from 14 to 40 kJ mol^{-1} [59]. This could imply that the ion-conduction mechanism in the membrane will be dominated by this mechanism. Hence, one hypothesis is that the SO_4H^- and $SO_4^{=}$ anions from the ionic liquid could interact with the PBI and displace the ion away from the exchange sites (N–H) of PBI and the ionic channel between PBI molecules, however this was not observed by FT-IR. Kreuer [60] suggested that the proton transport in acid-based materials under anhydrous or low humidity conditions occurs by a Grotthuss mechanism, in which only protons move from site to site without diffusible water molecules, such as H_3O^+ or $H_5O_2^+$. In this case the vehicular transport mechanism play a big role, when the amount of IL is increased in the PBI/*x*DESH, the ionic conductivity also consequently increased (see Fig. 5), but without excluding totally the hopping transport, it is possible to think that the vehicular transport will be dominant. The vehicular mechanism is also consistent with the observed IL drag/migration from anode to cathode in the fuel cell tests.

In the PBI/6DESH(2) sample, the specific conductivity was slightly higher than PBI/6DESH in the low temperatures (60 °C–120 °C) and more noticeably between 120 and 200 °C, (Fig. 5). The PBI/6DESH(2) membranes have more "free H_2SO_4 molecules" but these molecules cannot move effectively for a long distance. The ionic liquid thus forms an ionic channel within the polymer matrix to enhance the conductivity. Fig. 6 gives the schematic illustration of the PBI/*x*DESH ionic channel system hypothesis.

The obtained PBI/*x*DESH membranes could operate under a higher temperature/low humidity conditions with acceptable conductivity level >0.01 S cm^{-1}.

Table 2
The activation energy of PBI/DESH composite membranes obtained from ionic conductivity regression.

Sample	Slope log σ vs (1000/T) 60–120 °C/120–200 °C)	E_a(kJ mol^{-1}) 60–120 °C/120–200 °C dry/low humidity
PBI/12	–-1.675/-1.134	32.03 ± 0.26/21.7 ± 3.7
PBI/8	–1.434/–1.3429	27.42 ± 0.21/25.7 ± 1.4
PBI/6 (2)	–1.395/–1.441	26.69 ± 0.1/27.5 ± 2.7
PBI/6	–1.721/–1.228	32.91 ± 0.63/23.5 ± 2.7
PBI/4	–1.418/–1.288	27.12 ± 0.2/24.6 ± 1.4
PBI/3	–0.823/–1.054	15.74 ± 1.23/20.2 ± 2.0

3.3. Fuel cell performance

The need for good proton conduction without water transfer is particularly challenging. Besides that, in order to function as HT-PEMFC membranes, membranes need to satisfy other characteristics: low permeability to H_2 and O_2, thermal stability, dimensional stability with changes in temperature and hydration and

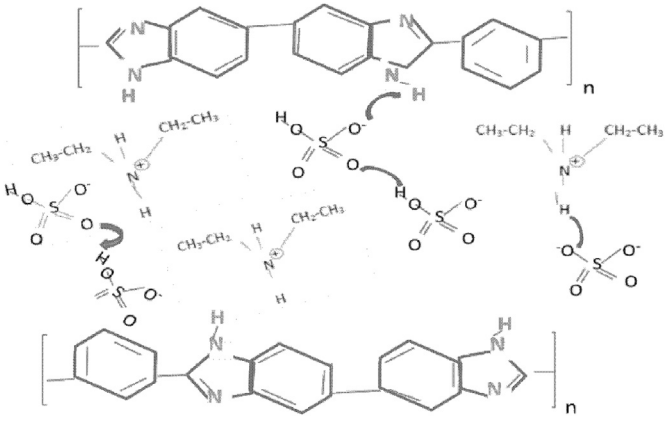

Fig. 6. Conduction model.

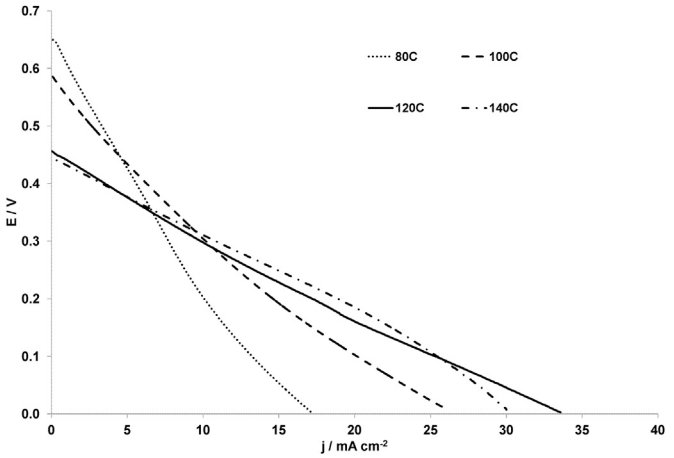

Fig. 7. Polarisation curves at 0.5 mV s^{-1} for PBI/8DESH at RH of 25, 47, 25 & 13% at 80, 100, 120 & 140 °C respectively.

electrochemical stability under reducing and oxidizing potentials in the presence of O_2 and H_2. The compatibility with the electrocatalyst in the fuel cell is also critical.

Under operational conditions, fuel cells have a voltage loss from three different sources: kinetics, Ohmic and mass transport losses. The Ohmic losses are related to the conductivity of the electrolyte, while mass transport losses will be affected by the electrode design and permeability of the IL. However, it is difficult to predict the cause of activation losses because it is very much dependent on the interfacial electrochemical interactions between the ions and the catalyst nanoparticles (electrode surfaces) as well as the compatibility/adsorption of the IL on the used catalyst surface. The activity of the proton produced in the HOR and consumed in the ORR strongly depends on the nature of the ionic liquid system involved.

Fig. 7 shows H_2/O_2 polarisation curves for PBI/8DESH at different temperatures. Increasing the temperature resulted in a decrease in the observed OCV from 0.66 to 0.45 V and improvement in the polarisation curve slope. The increase in the slope could be attributed to enhancement of proton diffusion. The increase in the measured ionic conductivity is clearly shown in Table 3. At a humidity of 25%, the resistivity decreased from ca. 8 to 3 Ω cm^2 when the temperature increased from 80 to 120 °C. Moreover, at fixed water vapour pressure (decreased humidity with increased temperature) the ionic resistivity decreased from 3.8 to 2.7 Ω cm^2 when the temperature increased from 100 to 140 °C. This corresponds to ionic conductivity (considering the membrane thickness of 224 μm) ca. $6 \times 10^{-3}$and 8.3×10^{-3} S cm^{-1} at 120 (RH 25%) and 140 °C (RH 13%), respectively. This agrees very closely with the ex-situ through plane membrane measurement of 7×10^{-3} and 1×10^{-2} S cm^{-1}, respectively at similar conditions. The beneficial effect of humidity on the ionic conduction in IL suggests that a further decrease in IL viscosity enhances the ions (H^+) and reactant diffusion.

To obtain the proton conductivity of IL, the proton transference number must be measured [61]. One of the best ways to do that is in symmetrical cells as reported for Li^+ IL [43,44]. In this work we applied a similar method using hydrogen, where H_2 is oxidized at the anode and re-generated (H_2 evolution) at the cathode. The measured slope of the *I–V* line is reported in Tables 3 and 4 as proton resistivity, R_{H^+}, and consequently the proton conductivity is calculated σ_{H^+}.

The measured proton conductivity, however, is ca. 4 times lower than that of the measured ionic conductivity (Table 3). This could be estimated roughly by considering Equation (3) for proton

Table 3
Through plane (MEA) ionic and protonic conductivity and resistivity for PBI/8DESH.

T °C	RH %	R_{onic}/FRA ohm cm^2	R_{H^+}/IV slope ohm cm^2	σ_{onic}/FRA S cm^{-1}	σ_{H^+}/IV slope S cm^{-1}	$\sigma_{onic}/\sigma_{H^+}$ –
80	25	8.06	–	0.0028	–	–
100	47	3.84	15	0.0059	0.0015	3.9
120	25	2.98	12.3	0.0075	0.0018	4.1
140	13	2.72	–	0.0083	–	–

conduction where the proton is associated with two anions A^- resulting in ionic agglomerate HA^{2-} with more than double the ionic radius of A^- and consequently less than half of its diffusion. Additionally, considering the solvation of that agglomerate (osmotic drag) with λ_{IL} estimated to be approximately 1 [62] will result in increase in the radius of the diffusing agglomerate further to reach 3–5 times the size of the initial A^- anion (depending on the size of the associated cation).

The low OCV could arise from the IL anion adsorption on the Nobel catalyst (Pt) or its electrochemical activity as an intermediate in Reactions (2) and (5) or due to mixed potential arising from electrochemical instability of the IL ions (reduced or oxidized). The strong adsorption of several IL has been reported on Au and Pt [30–32].

The very slow recovery in the OCV (in logarithmic behaviour) after a potential step (shown in Fig. 8) with time clearly indicates the slow adsorption of these reactants H_2, O_2, H^+ on the Pt surface due to IL ions strong adsorption or sluggish mixed potential equilibrium.

The adsorption of sulphate [63] and bisulphate [64] on platinum is also documented in the literature. Sulphuric acid based (PBI–H_2SO_4) H_2–O_2 fuel cell showed a decrease in OCV from 0.95 V at 80 °C to 0.67 V at 120 °C as the system lost water [15]. The OCV also decreased from 0.9 to 0.7 at 70 °C depending on dehydration of the PBI–sulphuric acid membrane (RH%) [65]. As the system dehydrates, ions adsorption will become stronger. Moreover, the possible effect of mixed potential at the anode and cathode will be signified with water loss and a temperature increase, as will be explained below.

Sulphuric acid is known to be reduced under fuel cell operating conditions [66]. Sulphate/bisulphate could undergo several electrochemical redox reaction, the following reactions can occur in H_2/O_2 fuel cell as they have equilibrium potential higher than the HOR and lower than the ORR [67,68]:

$$SO_4^{2-} + 4H^+ + 2e^- \leftrightarrow SO_2 + 2H_2O \quad E_r^0 = +0.138 \text{ vs. SHE at } 25\,^\circ\text{C} \tag{9}$$

$$SO_4^{2-} + 4H^+ + 2e^- \leftrightarrow H_2SO_3 + H_2O \quad E_r^0 = +0.17 \text{ vs. SHE at } 25\,^\circ\text{C} \tag{10}$$

$$HSO_4^- + 9H^+ + 8e^- \leftrightarrow H_2S(aq) + 4H_2O \quad E_r^0 = +0.289 \text{ vs. SHE at } 25\,^\circ\text{C} \tag{11}$$

$$SO_4^{2-} + 10H^+ + 8e^- \leftrightarrow H_2S(aq) + 4H_2O \quad E_r^0 = +0.303 \text{ vs. SHE at } 25\,^\circ\text{C} \tag{12}$$

Scott [69] studied Reaction (9) on platinum. Increasing sulphuric acid concentration caused an increase in over-potential for SO_2 oxidation. Operation at higher temperatures imposes practical problems of SO_2 loss from solution i.e. higher acid concentration, higher temperatures and lower H_2O will shift the equilibrium of Reactions 9–12 to the right towards reduction at the anode, while

Table 4
OCV, through plane (MEA) ionic and protonic conductivity and resistivity for PBI/6DESH(2).

T °C	RH %	R_{ionic}/FRA ohm cm^2	R_{H^+}/IV slope ohm cm^2	σ_{onic}/ FRA S cm^{-1}	σ_{H^+}/IV slope S cm^{-1}	E_{OCV} V	$\sigma_{onic}/\sigma_{H^+}$ –
18	100	–	–	–	–	980	–
18	0	23.54	–	0.0012	–	910	–
30	0	–	–	–	–	796	–
60	0	15.62	51.9	0.0017	0.00052	783	3.32
60	100	5.06	–	0.0052	–	829	–
80	100	0.78	–	0.034	–	800	–
100	47	10.4	32.9	0.0026	0.00082	715	3.16
150	10	13.92	52.8	0.0019	0.00051	660	3.79
180	5	9.18	–	0.0029	–	625	–
80	100	5.2	–	0.0054	–	810	–

the reverse (oxidation) will occur at the cathode causing mixed potential at both electrodes. The product H_2S, from Reactions (11) and (12), can absorb strongly on platinum leading to its poisoning [70].

Fig. 9 shows cell and anode polarisation curves for 6DEA-HSO_4 at 10%RH and 120 °C. The anode polarisation (including membrane IR) was obtained after purging the cell cathode first with argon and then with hydrogen. The anode polarisation was obtained with a H_2 feed at both the anode and cathode, with the anode as the working electrode (hydrogen oxidation) and the cathode as a counter and reference electrode (hydrogen evolution reaction (HER)). The obtained anode polarisation therefore also included the IR contribution from the membrane as well as a small contribution from the hydrogen evolution reaction (counter electrode). Large activation polarisation losses accompanied by a low observed limiting current of ca. 25 mA cm^{-2} can be seen from the anode polarisation. This suggests limited HOR on Pt in the used IL. While H_2 ionization is typically fast on Pt, sluggishness in Reaction (3) accompanied by slow HA_2^- (or $(CH_3CH_2)_2NH_2^+$ HA_2^-) diffusion could easily explain the observed anode response. The diffusion limiting species responsible for the observed limiting current is confirmed to be the hydrogen ion carrier species and not H_2 permeability in other IL systems([dema] cation) because of the IL weak activity as a proton donor [42].

Moreover, possible H_2S poisoning along with cation adsorption at the anode will hinder and slow considerably H_2 adsorption on Pt and consequently slow the HOR rate.

The low OCV of the cell at 0.8 V suggests mixed potential at the cathode (and anode). To further understand this, the cell potential was increased from 0.8 to 1.15 V (theoretical reversible potential for H_2/O_2 into steam). As a result an oxidative current increasing sharply with potential suggesting an oxidation reaction taking place at the cathode along with the ORR (and similarly reduction reaction occurring at the anode along with HOR) as discussed previously in Reactions (6)–(9). The rate of this redox reaction is considerable and reached a value of 13 mA cm^{-2} at 1.15 V in comparison to the observed limiting current density of 25 mA cm^{-2}.

Fig. 10 shows cell polarisation curves for PBI/6DESH(2)at RH of 100, 100, 47, 10 & 5% at 60, 80, 100, 150 & 180 °C respectively. The cell polarisation data for the PBI-5.6H_3PO_4 system using similar electrodes, from our previous work, is also provided for comparison [71]. As expected the PBI–H_3PO_4 system showed superior performance to that of the PBI-IL system. This was caused by the low H_2/O_2 permeability of the IL in comparison to H_3PO_4 as demonstrated by the very low observed limiting current (in the IL system) and partially by the lower conductivity of the PBI-IL system. For example at 150 °C, with oxygen, no limiting current was observed for the PBI–H_3PO_4 system at the investigated current densities up to 2.5 A cm^{-2} [71] in comparison with 8 mA cm^{-2} with IL.

The strong dependence of the recorded OCV with water content is shown in Table 4. As the water content decreased or temperature increased, the OCV fell sharply. This behaviour is reversible as the OCV recovered after a decrease in temperature or an increase in RH. For example at fixed temperature, the OCV decreased from 980 to 910 mV and from 829 to 783 mV when the RH was changed from 100 to 0% at 18 and 60 °C, respectively. Similar data can be found in the literature for PBI–sulphuric acid membrane, OCV also decreased from 0.9 to 0.7 at 70 °C depending on dehydration of the

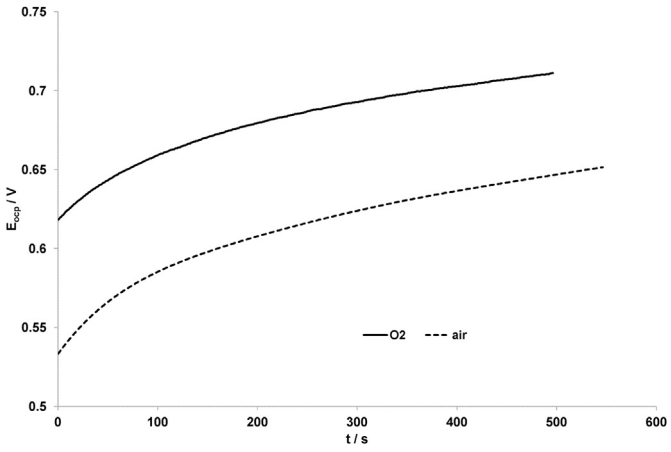

Fig. 8. PBI/8DESH OCV vs time at 0%RH at 60 °C.

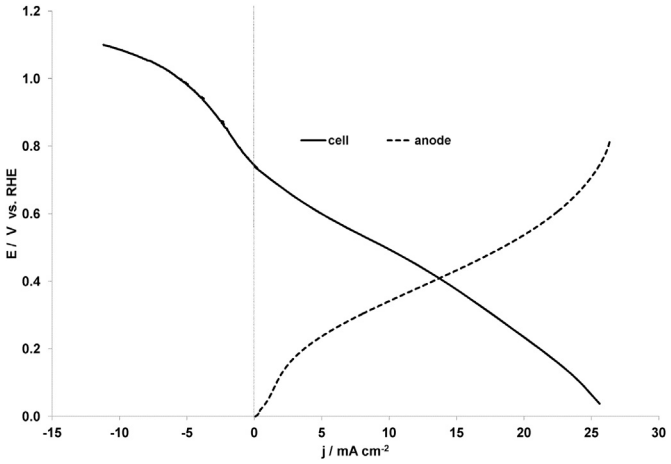

Fig. 9. Cell and anode polarisation curves at 0.5 mV s^{-1} for PBI/6DESH at 10%RH and 120 °C.

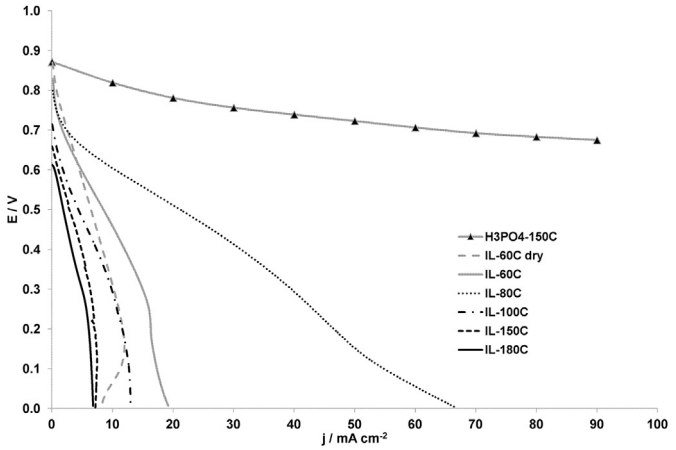

Fig. 10. Polarisation curves at 0.5 mV s^{-1} for PBI-5.6H_3PO_4 (at 150 °C) and PBI/6DESH(2) at RH of 100, 100, 47, 10 & 5% at 60, 80,100, 150 & 180 °C respectively.

(RH%) [65]. OCV of 0.5–0.62 V was reported for porous PBI film with 1-H-3-methylimidazolium bis(trifluoromethanesulphonyll)imide using 5 mg_{pt} cm^{-2} at 1.5 atm pressure and temperature range of 30–150 °C [37]. Similarly the OCV is reported to fall from 0.9 to 0.6 V when temperature was increased from 80 to 120 °C in N-ethyl-N-methylpyrrolidinium fluorohydrogenate (1 mg_{Pt} cm^{-2}) [35] and ca. 0.7 V at 140 °C for a fuel cell utilizing diethylmethylammonium trifluoro-methanesulphonate [dema][TfO] [24]. As mentioned earlier this is explained by a shifting in the equilibrium of Reactions (9)–(12) (mainly (11)) towards increasing rate in H_2S production at the anode (opposite at the cathode) with a more significant mixed potential effect.

The beneficial effect of humidity on the decrease of the IL viscosity can also be seen from the polarisation curves. This can be explained by reduction in the IL viscosity and improvement in the H^+ and H_2 and O_2 diffusion. Optimum performance under a fixed water content (humidifier at 80 °C, 100% RH at 80 °C) is observed at 80 °C with no limiting current and maximum current density of ca 70 mA cm^{-2}.

As the system temperature increased beyond 80 °C and the system starts to dehydrate, the IL viscosity starts to increase and proton diffusion is hindered (lower ionization reflected in large decrease in ionic conductivity). This is reflected in limiting current densities of 13 and 8 mA cm^{-2} at 100 and 150 °C, respectively. Under humidified conditions, optimum hydration rate and consequently highest ionic conductivity is achieved at 80 °C (Table 4). The through plane ionic resistivity decreased to a minimum of 0.78 Ω cm^{-2}, which corresponds to ionic conductivity of 0.034 S cm^{-1} (100% RH) considering a membrane thickness of 270 μm. However, as the temperature reached 100 °C, while maintaining the water vapour pressure, the system dehydrated significantly even at high humidity (47%) and the ionic conductivity decreased by an order of magnitude to 0.0026 S cm^{-1}. The measured proton conductivity is ca. 3–4 times lower than that of the measured ionic conductivity in accord with the values measured and shown in Table 3.

The ionic conductivity above 100 °C didn't change significantly. However, values of the through plane ionic conductivity measured in the MEA were lower than those measured ex-situ for the membrane at temperatures above 100 °C. Ex-situ measurement showed ca. 4 times higher ionic conductivities of 8×10^{-3} and 10^{-2} at 150 and 180 °C, respectively (at same RH). This can be explained by the migration of the IL from anode to cathode due to osmotic drag.

The mentioned (hydro-dynamical) solvation phenomenon is well known in PEMFCs as the proton water osmotic drag, with typical values of coefficient in the range 1.5–2.8 for Nafion [72]. Water dragged with protons from PEMFC anode to cathode does not generally create serious flooding problem as water will vaporise at the cathode and move with exist gases. However, in an IL environment, as the IL is non-volatile with a high boiling point, the hydro-dynamical solvation will not only lead to slower proton diffusion and consequently lower conductivity but also will cause serious flooding and mass transport limitation at the cathode. This cumulative effect will limit the life of the cell due to the IL migration from anode and membrane to the cathode. IL fuel cell's under current flow showed non homogenous distribution of IL, with true migration of IL towards the cathode induced by electro-osmotic drag with λ_{IL} estimated to be approximately 1 [62].

Post-mortem SEM studies were conducted on the MEAs electrodes' after the PEMFC evaluation testing in order to corroborate the migration of IL from anode to cathode. Fig. 11a shows the SEM image from cathode GDL (carbon cloth), the structure appears flooded with IL in comparison to the anodic GDL (Fig. 11b). The weight increase for the cathode GDL after operation was 36 wt% in comparison to 19% for the anode GDL. This was obtained by recording the weight difference after boiling the tested electrodes in DI (to remove the migrated IL) water and drying in oven.

The migration of the IL to the electrodes and particularly from anode/membrane to cathode will reduce the content of the IL in the membrane when the MEA is under polarisation (current flow). This was confirmed by re-measuring the ionic conductivity of the MEA after it was cooled to 80 °C. The cell ionic resistivity increased by a factor of approximately 6 times before and after polarisation/

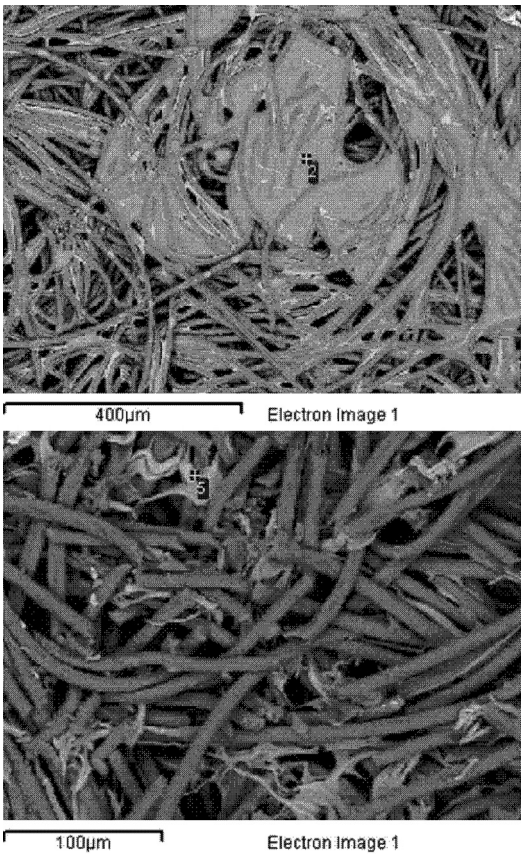

Fig. 11. SEM of GDL from PEM PBI/8DESH, carbon cloth. A) Cathode (top), B) Anode (bottom).

heating cycle with a value of 0.78 at the start and 5.2 Ω cm^2 at the end of the experiment.

4. Conclusion

Diethlyamine bisulphate/sulphate ionic liquid was synthesised and characterised for high temperature fuel cell application. Composite hybrid membranes of PBI and ionic liquid diethlyamine bisulphate/sulphate were fabricated at different composition ratios PBI/*x*DESH. The ratio diethylamine/sulphuric acid was 1/1 mol DESH or 1/2 mol DESH(2).

Results from elemental analysis suggest that the ionic liquid DESH or DESH(2), does not only contain the anion bisulphate (SO_4H^-), but rather we could think of it as a mixture of bisulphate and sulphate anions. The experimental S/N ratios obtained were 1.51 to (DESH) and 1.68 to (DESH(2)), suggesting a mixture of both anions is present. Similarly results from ^1H NMR suggested a mixture of both anions with the integration of the H peak the bisulphate anion spectrum less than one.

FTIR spectra of the ionic liquid incorporated in PBI showed that the IL did not change the PBI structure. The imine group from the imidazole ring was not protonated, and the ionic liquid only weakly interacts with PBI and remains free inside the structure of PBI film allowing for the observed ionic conduction.

PBI/*x*DESH membranes could operate under a higher temperature/low humidity conditions with acceptable conductivity level >0.01 S cm^{-1} for membranes with doping level of 6PRU ($x = 6$) and above.

The measured proton conductivity obtained from symmetrical H_2 cell, however, is ca. 4 times lower than that of the measured ionic conductivity. This could be estimated roughly by considering proton conduction, where the proton is associated with two anions A^- resulting in an ionic agglomerate HA^{2-} with more than double the ionic radius of A^- and consequently less than half its diffusivity. Additionally, considering the solvation of that agglomerate (osmotic drag) with λ_{IL} estimated to be approximately 1 will result in an increase in the radius of the diffusing agglomerate to reach 3–5 times the size of the initial A^- anion (depending on the size of the associated cation). The mentioned (hydro-dynamical) solvation phenomenon is well known in PEMFCs as proton water osmotic drag coefficient, with typical values in the range 1.5–2.8 for Nafion [72]. Water dragged with protons from PEMFC anode to cathode doesn't generally create serious flooding problem as water will vaporise at the cathode and move with exist gases. However, in IL environment as IL is a non-volatile compound with high boiling point, the hydro-dynamical solvation will not only lead to slower proton diffusion and consequently lower conductivity but also will cause serious flooding and mass transport limitation at the cathode. This cumulative effect will limit the life of the cell due to the IL migration from anode and membrane to the cathode.

The low OCV of the cell at 0.8 V suggests a mixed potential at the cathode (and anode). An oxidation reaction takes place at the cathode along with the ORR (and similarly reduction reaction occurring at the anode along with HOR) as discussed previously in Reactions (6)–(9) along with the poisoning effect of H_2S generated at the anode on Pt. The rate of this redox reaction was considerable and reached a value of 13 mA cm^{-2} at 1.15 V in comparison to the observed limiting current of 25 mA cm^{-2}.

The beneficial effect of humidity on the decrease of the IL viscosity was observed in the fuel cell polarisation curves. This can be explained by reduction in the IL viscosity and improvement in the H^+ and H_2 and O_2 diffusion. Optimum performance under fixed water content (humidifier at 80 °C, 100% RH at 80 °C) is observed at 80 °C with no limiting current and maximum current density of ca 70 mA cm^{-2}.

As the system temperature increased beyond 80 °C, the system starts to dehydrate. This was reflected in limiting current of 13 and 8 mA cm^{-2} at 100 and 150 °C, respectively.

Acknowledgements

The authors acknowledge the support of the EPSRC for funding under the SUPERGEN Fuel Cells consortia. The authors also like to acknowledge the support of funding from Spain under project CTQ2010-17338 and S2009/ENE-1743.

References

[1] O. Savadogo, Journal of New Materials for Electrochemical Systems 1 (1998) 47–66.
[2] B. Smitha, S. Sridhar, A.A. Khan, Journal of Membrane Science 259 (2005) 10–26.
[3] J. Schauer, Current Trends in Polymer Science 10 (2006) 19–26.
[4] F. de Bruijn, Green Chemistry 7 (2005) 132–150.
[5] B.C.H. Steele, A. Heinzel, Nature 414 (2001) 345–352.
[6] N. Agmon, Chemical Physics Letters 244 (1995) 456–462.
[7] K.D. Kreuer, Journal of Membrane Science 185 (2001) 29–39.
[8] M. Saito, K. Hayamizu, T. Okada, The Journal of Physical Chemistry B 109 (2005) 3112–3119.
[9] M. Mamlouk, K. Scott, Electrochimica Acta 56 (2011) 5493–5512.
[10] S.J. Peighambardoust, S. Rowshanzamir, M. Amjadi, International Journal of Hydrogen Energy 35 (2010) 9349–9384.
[11] Q.F. Li, J.O. Jensen, R.F. Savinell, N.J. Bjerrum, Progress in Polymer Science 34 (2009) 449–477.
[12] J. Lobato, P. Canizares, M.A. Rodrigo, J.J. Linares, J.A. Aguilar, Journal of Membrane Science 306 (2007) 47–55.
[13] M. Mamlouk, K. Scott, Journal of Fuel Cell Science and Technology 8 (2011).
[14] M. Martinez, Y. Molmeret, L. Cointeaux, C. Iojoiu, J.C. Lepretre, N. El Kissi, P. Judeinstein, J.Y. Sanchez, Journal of Power Sources 195 (2010) 5829–5839.
[15] X. Wu, K. Scott, Fuel Cells 12 (2012) 583–588.
[16] M. Mamlouk, K. Scott, Proceedings of the Institution of Mechanical Engineers, Part A Journal of Power and Energy 225 (2011) 161–174.
[17] G. Alberti, M. Casciola, L. Massinelli, B. Bauer, Journal of Membrane Science 185 (2001) 73–81.
[18] M. Mamlouk, K. Scott, Journal of Power Sources 196 (2011) 1084–1089.
[19] K.D. Kreuer, A. Fuchs, M. Ise, M. Spaeth, J. Maier, Electrochimica Acta 43 (1998) 1281–1288.
[20] Q.T. Che, R.H. He, J.S. Yang, L. Feng, R.F. Savinell, Electrochemistry Communications 12 (2010) 647–649.
[21] C.A. Angell, W. Xu, J.P. Belieres, M. Yoshizawa, U.S. Patent, Arizona Board of Regents for and on Behalf of Arizona State University, USA, 2011.
[22] K. Ueno, H. Tokuda, M. Watanabe, Physical Chemistry Chemical Physics 12 (2010) 15133–15134.
[23] E. Cho, J.S. Park, S.S. Sekhon, G.G. Park, T.H. Yang, W.Y. Lee, C.S. Kim, S.B. Park, Journal of the Electrochemical Society 156 (2009) B197–B202.
[24] S.-Y. Lee, A. Ogawa, M. Kanno, H. Nakamoto, T. Yasuda, M. Watanabe, Journal of the American Chemical Society 132 (2010) 9764–9773.
[25] J. Kielland, Journal of Chemical Education 14 (1937) 412.
[26] J.F. Hinton, E.S. Amis, Chemical Reviews 71 (1971) 627–674.
[27] R. Gopal, O.N. Bhatnagar, The Journal of Physical Chemistry 69 (1965) 2382–2385.
[28] U.A. Rana, M. Forsyth, D.R. MacFarlane, J.M. Pringle, Electrochimica Acta (2012).
[29] C.M. Ó'Laoire, Northeastern University, PhD thesis, Boston, 2010.
[30] F. Endres, O. Hofft, N. Borisenko, L.H. Gasparotto, A. Prowald, R. Al-Salman, T. Carstens, R. Atkin, A. Bund, S. Zein El Abedin, Physical Chemistry Chemical Physics 12 (2010) 1724–1732.
[31] S. Mitsushima, Y. Hata, K. Muneyasu, N. Kamiya, K.I. Ota, Journal of New Materials for Electrochemical Systems 10 (2007) 61–65.
[32] R. Hayes, N. Borisenko, M.K. Tam, P.C. Howlett, F. Endres, R. Atkin, The Journal of Physical Chemistry C 115 (2011) 6855–6863.
[33] R. Hagiwara, T. Nohira, K. Matsumoto, Y. Tamba, Electrochemical and Solid-State Letters 8 (2005) A231–A233.
[34] M.A.B.H. Susan, A. Noda, S. Mitsushima, M. Watanabe, Chemical Communications 9 (2003) 938–939.
[35] P. Kiatkittikul, T. Nohira, R. Hagiwara, Journal of Power Sources 220 (2012) 10–14.
[36] A. Noda, M.A.B. Susan, K. Kudo, S. Mitsushima, K. Hayamizu, M. Watanabe, The Journal of Physical Chemistry B 107 (2003) 4024–4033.
[37] E. van de Ven, A. Chairuna, G.r. Merle, S.P. Benito, Z. Borneman, K. Nijmeijer, Journal of Power Sources 222 (2013) 202–209.
[38] S.S. Sekhon, B.S. Lalia, J.S. Park, C.S. Kim, K. Yamada, Journal of Materials Chemistry 16 (2006) 2256–2265.
[39] D. Inoue, S. Mitsushima, K. Matsuzawa, S.Y. Lee, T. Yasuda, M. Watanabe, K.I. Ota, Electrochemistry 79 (2011) 377–380.

[40] T. Sakai, H. Takenako, N. Wakabayashi, Y. Kawami, E. Torikai, Journal of The Electrochemical Society 132 (1985) 1328.
[41] R.H. He, Q.F. Li, A. Bach, J.O. Jensen, N.J. Bjerrum, Journal of Membrane Science 277 (2006) 38–45.
[42] S. Mitsushima, Y. Shinohara, K. Matsuzawa, K.I. Ota, Electrochimica Acta 55 (2010) 6639–6644.
[43] J.W. Park, K. Yoshida, N. Tachikawa, K. Dokko, M. Watanabe, Journal of Power Sources 196 (2010) 2264–2268.
[44] N. Tachikawa, J.W. Park, K. Yoshida, T. Tamura, K. Dokko, M. Watanabe, Electrochemistry 78 (2010) 349–352.
[45] J.S. Baek, J.S. Park, S.S. Sekhon, T.H. Yang, Y.G. Shul, J.H. Choi, Fuel Cells, 10 762–769.
[46] X. Xuew, M. Kanzaki, Journal of the American Ceramic Society 92 (2009) 2803–2830.
[47] P. Musto, F.E. Karasz, W.J. Macknight, Polymer 34 (1993) 2934–2945.
[48] P. Musto, F.E. Karasz, W.J. Macknight, Polymer 30 (1989) 1012–1021.
[49] R. Bouchet, E. Siebert, Solid State Ionics 118 (1999) 287–299.
[50] J.A. Asensio, E.M. Sanchez, P. Gomez-Romero, Chemical Society Reviews 39 (2010) 3210–3239.
[51] A. Goypiron, J. de Villepin, A. Novak, Spectrochimica Acta Part A: Molecular Spectroscopy 31 (1975) 805–818.
[52] W. Xu, E.I. Cooper, C.A. Angell, The Journal of Physical Chemistry B 107 (2003) 6170–6178.
[53] M. Yamada, I. Honma, Electrochimica Acta 48 (2003) 2411–2515.
[54] M.L. Hoarfrost, M.S. Tyagi, R.A. Segalman, J.A. Reimer, Macromolecules 45 (2012) 3112–3120.
[55] M. Mamlouk, K. Scott, International Journal of Energy Research 35 (2011) 507–519.
[56] M.C. Wintersgill, J.J. Fontanella, Electrochimica Acta 43 (1998) 1533–1538.
[57] A.P. Abbott, ChemPhysChem 5 (2004) 1242–1246.
[58] P. Wasserscheid, in: T. Welton (Ed.), Ionic Liquids in Synthesis, vol. 2, 2003.
[59] J.T.-W. Wang, S.L.-C. Hsu, Electrochimica Acta 56 (2011) 2842–2846.
[60] K.D. Kreuer, Chemistry of Materials 8 (1996) 610.
[61] H. Nakamoto, M. Watanabe, Chemical Communications 24 (2007) 2539–2541.
[62] A. Martinelli, C. Iojoiu, N. Sergent, Fuel Cells 12 (2012) 169–178.
[63] S. Schuldiner, M. Rosen, Journal of The Electrochemical Society 118 (1971).
[64] S. Thomas, Y.-E. Sung, H.S. Kim, A. Wieckowski, The Journal of Physical Chemistry 100 (1996) 11726–11735.
[65] O. Savadogo, B. Xing, Journal of New Materials for Electrochemical Systems 3 (2000) 345–349.
[66] G.V. Elmore, H.A. Tanner, Journal of The Electrochemical Society 108 (1961) 669–671.
[67] M. Bouroushian, Electrochemistry of Metal Chalcogenides, vol. XII, Springer, 2010.
[68] T.P. Goldstein, Z. Aizenshtat, Journal of Thermal Analysis 42 (1994) 241–290.
[69] K. Scott, W.M. Taama, Electrochimica Acta 44 (1999) 3421–3427.
[70] R. Mohtadi, W.-k. Lee, S. Cowan, J.W.V. Zee, M. Murthy, Electrochemical and Solid-State Letters 6 (2003) A272–A274.
[71] M. Mamlouk, K. Scott, International Journal of Hydrogen Energy 35 (2010) 784–793.
[72] B.S. Pivovar, Polymer 47 (2006) 4194–4202.